Glass-Like Characteristics of Intracellular Motion in Human Cells

Åberg, Christoffer; Poolman, Bert

IMPORTANT NOTE: You are advised to consult the publisher's version (publisher's PDF) if you wish to cite from it. Please check the document version below.

Document Version
Publisher's PDF, also known as Version of record

[Link to publication in University of Groningen/UMCG research database](#)

Glass-like characteristics of intracellular motion in human cells

Christoffer Åberg[1,2,*] and Bert Poolman[2]
[1]Groningen Research Institute of Pharmacy, University of Groningen, Groningen, the Netherlands and [2]Department of Biochemistry, Groningen Biomolecular Sciences and Biotechnology Institute, University of Groningen, Groningen, the Netherlands

ABSTRACT The motion in the cytosol of microorganisms such as bacteria and yeast has been observed to undergo a dramatic slowing down upon cell energy depletion. These observations have been interpreted as the motion being "glassy," but whether this notion is useful also for active, motor-protein-driven transport in eukaryotic cells is less clear. Here, we use fluorescence microscopy of beads in human (HeLa) cells to probe the motion of membrane-surrounded structures that are carried along the cytoskeleton by motor proteins. Evaluating several hallmarks of glassy dynamics, we show that at short length scales, the motion is heterogeneous, is nonergodic, is well described by a model for the displacement distribution in glassy systems, and exhibits a decoupling of the exchange and persistence times. Overall, these results suggest that the short length scale behavior of objects that can be transported actively by motor proteins in human cells shares features with the motion in glassy systems.

SIGNIFICANCE Recent reports have suggested an analogy between the motion inside cells and that in "glassy" systems. The motion in a glass, itself not completely understood, is often characterized in terms of objects remaining stationary for extended periods of time, only infrequently being able to move longer distances. Whether such a behavior is observed also for objects that can move actively along the cytoskeleton through the action of motor proteins is less clear. Here, we test this hypothesis, and we show that the motion of objects that can be transported actively by motor proteins in human cells exhibits several features that are typical of that in glassy systems.

INTRODUCTION

The living cell is a highly complex nonequilibrium system composed of a multitude of interacting units at several length scales and timescales. The motion of molecules, macromolecular complexes, and organelles within and on the cell surface has captured the eye of physicists as examples of random motion that (often) defies the classical paradigm set by Brownian motion (1,2). Partly, this interest certainly stems from developments in methodology, being driven by the possibility of readily observing the dynamics of micron or nanosized particles (3–8) and even single molecules (9–11) by optical microscopy. Other aspects to the problem originate from analogies with soft matter science, including with colloidal glasses (12–15) and other complex systems (16,17).

In this context, the idea that intracellular motion is "glassy" has recently received attention (10). We use this term broadly to signify that the motion exhibits features that are characteristic of systems close to (but not necessarily at or beyond) a glass transition (16,17). We also emphasize that we do not imply that the mechanisms underlying the behavior are the same, just the observed features of the motion. The notion that cells exhibit glassy behavior is not entirely new; Janmey and MacKintosh (18) cite observations from more than a century ago alluding to glassy behavior, and one can also find more explicit comparisons in the fairly recent literature (7,19,20). For example, the motion at the 1–100-s timescale of insulin granules in MIN6 mouse cells is nonergodic and exhibits a decoupling of exchange and persistence times (7), both characteristics of glassy motion. The motion of colloidal beads on lipid bilayer tubes, although not strictly related to intracellular motion, also exhibit a decoupling of exchange and persistence times (19). Furthermore, while on the cell exterior, the motion of beads on the membrane of human airway smooth muscle cells has also been interpreted in terms of glassy dynamics (20). In

microorganisms, an interesting observation is that the type of motion appears to be highly sensitive to control parameters. Thus, the motion of molecular complexes in *Escherichia coli* cells has been interpreted as glassy only in the absence of cell energy, whereas in its presence, the motion becomes diffusive, the cell being "fluidized" by metabolic activity (10). In *Saccharomyces cerevisiae* cells, a qualitative change in motion of molecular complexes (11,21,22) has been linked to a change in pH (11) and/or macromolecular crowding (21).

For intracellular motion in general, it is important to distinguish between motor-protein-driven transport and "free" diffusion in the cytosol. Motor proteins expend cell energy to carry membrane-surrounded structures (vesicles and organelles) along the cytoskeleton. In contrast, when molecules and other objects are present in the cytosol, though obstructed by the cytoskeleton, organelles, vesicles, and the high degree of macromolecular crowding, they are free to move around, and their motion is not (directly) driven by motor proteins and is nondirectional. It is possible that an object being moved by motor proteins intermittently detaches from the cytoskeleton and subsequently moves freely in the cytosol before attaching again, so objects known to be transported by motor proteins could exhibit both types of motion. Eukaryotic cells, including mammalian and yeast, have both types of motion, whereas bacteria lack motor proteins such as myosin, kinesin, and dynein. Still, the simplicity of transport in bacteria should not be overemphasized, for there are multiple intracellular transport processes that are actively driven (23).

The revived interest in glassy characteristics of intracellular motion has been focused on cytosolic motion; here, we instead focus on motion that can occur by motor proteins and specifically in human cells. We use a standard human cell line (HeLa) to allow potential links to the wealth of biological information available for these cells. As probes for the transport, we use nanosized beads because they are readily taken up by cells (24,25) and are subsequently transported around the cell within membrane-surrounded structures by motor proteins (24–28). It also allows us to take advantage of our previous experience with how these beads interact with human cell systems (25,27–31). We focus on relatively short length scales because we hypothesize that glassy motion is here more likely to be a useful analogy. Using this model system, we test several hallmarks of glassy motion to evaluate to what extent the intracellular motion exhibits similar behavior: we evaluate the shape of the displacement distribution (self-part of the van Hove function (16)), whether the motion breaks ergodicity (weakly) (32), and a potential decoupling of the persistence and exchange times (33,34).

MATERIALS AND METHODS

Experimental procedure

HeLa cells were cultured at 37°C under a humidified atmosphere containing 5% CO_2 in Dulbecco's Modified Eagle's Medium containing UltraGlut-amine and 4.5 g/L glucose (Lonza, Verviers, Belgium) with 10% fetal bovine serum (GE Healthcare, Hoevelaken, the Netherlands) and were typically subcultured thrice weekly. For the experiments, 70,000 cells were seeded onto petri dishes with glass-bottom microwells (MatTek, Ashland, MA) and incubated further for at least a day. 40-nm yellow/green carboxylated polystyrene beads (Life Technologies, Carlsbad, CA) were dispersed in the cell growth medium. The beads were exposed to the cells by removal of the cell medium and subsequent addition of the bead suspension followed by 2 mL of fresh medium to the petri dish, both added away from the observation area, for a final concentration of 1 μg/mL. The cells were further incubated for 10 min, after which they were washed four times with 2 mL of fresh medium and further incubated for at least 5 h at 37°C under a humidified atmosphere containing 5% CO_2.

Microscopy was carried out on a homebuilt setup based upon an Olympus IX71 S1F-3 microscope (Olympus Life Science, Tokyo, Japan). To keep the temperature, a heating insert (PeCon, Erbach, Germany) was used. The beads were excited by a 488-nm laser (Coherent, Santa Clara, CA), whereas a halogen lamp was used for brightfield images. A 60× oil immersion objective (Apo N, N.A. 1.49; Olympus, Center Valley, PA) was used, together with an additional 1.6× magnification from the lens built into the microscope. Images were captured by a Hamamatsu EM-CCD digital camera (model no. 09100-13; Hamamatsu, Hamamatsu City, Japan) using MetaVue 7.7.0.0 (Molecular Devices, Sunnyvale, CA).

Tracking

Beads in focus were tracked using the TrackMate plugin (version 2.8.1) (35) available in the Fiji distribution (36) of ImageJ (37). For bead identification, we used the difference of Gaussian segmentation method with subpixel localization (35). For trajectory identification, we used the simple linear assignment problem tracker (35), allowing gaps of up to 10 frames (corresponding to roughly 310 ms) and five pixels (corresponding to roughly 0.8 μm). We chose these rather liberal settings to capture also far-moving trajectories. However, to avoid spurious trajectories, we manually checked all trajectories and only kept trajectories we were confident were correct; similarly, we also linked trajectories we were confident had been misidentified as being separate ones. Trajectories outside the cell or on what we presume to be the outer cell membrane were removed.

Analysis

For the lag-time-averaged mean-square displacement of a given trajectory, we calculated the displacement squared in two dimensions between all pairs of time points for which the trajectory is defined. The data were subsequently binned by lag time, using the average frame rate as bin size. The prefactor, Γ, and exponent, α, of a power law

$$\langle r^2 \rangle (\tau) = \Gamma \tau^{\alpha}, \qquad (1)$$

were extracted from the lag-time-averaged mean-square displacement in the interval 0.7–4 s by fitting a straight line to the logarithm of the mean-square displacement versus the logarithm of lag time. Trajectories with an R^2 from the fit <0.9 were ignored.

The lag-time- and ensemble-averaged mean-square displacement was evaluated by averaging the lag-time-averaged mean-square displacement over all trajectories.

To separate active and passive motion states, we calculated the lag-time-averaged mean-square displacement within a limited time window (eight frames, corresponding to around 250 ms). This was done for each point along the trajectory except the last ones (the last eight ones, for which the time window decreases successively). The mean-square displacement was then fitted to a power law (Eq. 1), and the R^2 of the fit recorded together with the fitting parameters.

To quantify the degree of ergodicity breaking, we adopted the parameter (38–40)

$$EB(\tau) = \lim_{t \to \infty} \frac{\langle X^2 \rangle - \langle X \rangle^2}{\langle X \rangle^2} = \lim_{t \to \infty} EB_t(\tau).$$ (2)

Here, $X(\tau; t)$ is the mean-square displacement of an individual trajectory, averaged over lag time, τ, up until time, t. Furthermore, here specifically, we denote an average over all trajectories (ensemble average) by $\langle ... \rangle$. Strictly speaking, we cannot calculate the infinite time limit in Eq. 2. Instead, we define a quantity, $EB_t(\tau)$, that tends to the ergodicity breaking parameter, $EB(\tau)$, as time tends to infinity. This quantity was calculated as a function of time as follows: each trajectory was "cut off" at the given time, the square displacement averaged over lag time was calculated for each resulting trajectory (X in Eq. 2), the relevant ensemble averages ($\langle ... \rangle$ in Eq. 2) were calculated, and the quantity, EB_t, was finally determined.

For the displacement distribution, all "subtrajectories" formed from the original trajectories by considering each point along the trajectory as a new trajectory, was used. Time was binned using the average frame rate as bin size. The (radial) displacements were calculated in two dimensions, after which their histogram was computed and normalized to yield the self-part of the van Hove function, $G_s(\Delta r; \tau)$. The normalization used was such that $G_s(\Delta r; \tau)2\pi\Delta r$ integrated over all Δr is unity.

The test whether the displacement distribution could be described by a Gaussian, we fitted the function

$$A\exp\left(-\Delta r^2 / 4D\tau\right),$$ (3)

to the data for $\Delta r < 0.25$ μm. To test if the data could be described by the Chaudhuri et al. model (41,42), we implemented their model according to Eq. S8, evaluating the integral numerically using the "quad" function of the "integrate" package of the python library scipy (43) version 0.19.1, together with numpy (44) version 1.19.4. When performing the fit, the model was fitted to the logarithm of the displacement distributions evaluated for all reported times simultaneously and with four free parameters (l, d, τ_1, and τ; see Supporting materials and methods). To test whether the data were well described by a pure exponential decay, we fitted the function

$$Ae^{-\Delta r/\lambda(\tau)},$$ (4)

where $\lambda(\tau)$ is a lag-time-dependent length scale to the data. We performed the fit on the logarithm of the displacement distribution and for Δr in the interval 0.1–0.4 μm.

The persistence and exchange times were calculated as outlined by Wang et al. (19). Briefly, to gain statistics, we used all "subtrajectories" formed from the original trajectories by considering each point along the trajectory as a new trajectory. We only considered (sub)trajectories that lasted at least 10 s and only considered the first 10 s in order not to introduce bias. The persistence time was defined as the first time the particle moved longer than the distance of interest within the (sub)trajectory; the exchange time was defined as the second time the particle moved longer after first having done so once. We refer to Wang et al. (19) for a more detailed discussion.

RESULTS AND DISCUSSION

We probed intracellular motion in HeLa (adenocarcinomic human cervical epithelial) cells using commercially available 40-nm (nominal diameter) carboxylated polystyrene beads. These beads are labeled in the core with multiple fluorophores and thus exhibit high fluorescence, are not expected to self-quench or Förster resonance energy transfer, and do not leach the fluorescent label significantly (25);

indeed, in our experience, their fluorescence is strong and stable (27,28,31). Furthermore, the beads do not degrade inside or cause damage to the cells (30). Crucially, the beads are readily taken up by cells by endocytic processes (24,25,45), implying that they subsequently remain within membrane-surrounded structures (25,26,46) rather than access the cytosol. The beads follow the endolysosomal pathway (47), where they are trafficked from organelles called early endosomes to late endosomes and ultimately to lysosomes, the degradative compartments of the cell that measure around 0.2 μm in radius (48). We waited an appropriate time to ensure that the beads had time to accumulate in the lysosomes, their predominant final location (25–28,30); however, some beads may reach other structures inside the cell, as yet unidentified but motile and separate from larger structures such as the endoplasmic reticulum, Golgi apparatus, or nucleus (26). There is no evidence that the beads exit from membrane-surrounded compartments, so the beads thus serve as probes of membrane-surrounded structures, most of them being lysosomes.

Aside from their fluorescent properties, using beads rather than labeling an organelle directly has the advantage that we can control the number of beads internalized by the cells (by changing the concentration). Thereby, we can limit the number of objects we have to follow and distinguish inside a given cell and hence improve trajectory identification. This is of particular importance when imaging cells in two dimensions, as done here to gain speed.

The cells were cultured on glass and exposed to a 10-min "pulse" of a 1 $\mu g/mL$ bead dispersion, after which the excess of beads was washed away. The cells were left to internalize and traffick the beads for at least 5 h before observation, at which point lysosomal accumulation is expected to be concluded (26). The cells were examined using (widefield) fluorescence microscopy, typically acquiring 1000 images roughly every 31.3 ms. The raw data are thus, in essence, "movies" of beads within cells in two dimensions. Fig. 1 a shows an example image from one of these "movies."

Open-source software was used to identify and locate the beads in each image, track them throughout the images of the "movie," and thereby form their trajectories. Data were acquired for several cells and later pooled together. The results presented here are based on 157 trajectories, most of them followed throughout the full "movie," though some trajectories are shorter (Fig. S1) either because of the bead disappearing from the observation volume and/or because identification worsened.

Two example trajectories are shown in Fig. 1 a, overlaid on the image that shows the initial positions of the beads, and at a higher magnification in Fig. 1 b. One of the beads (Fig. 1, a and b, $blue$) barely moves at all during the time course of this movie. Whether this bead resided in a membrane-surrounded structure that has detached from the cytoskeleton, if it was obstructed from moving or did not move
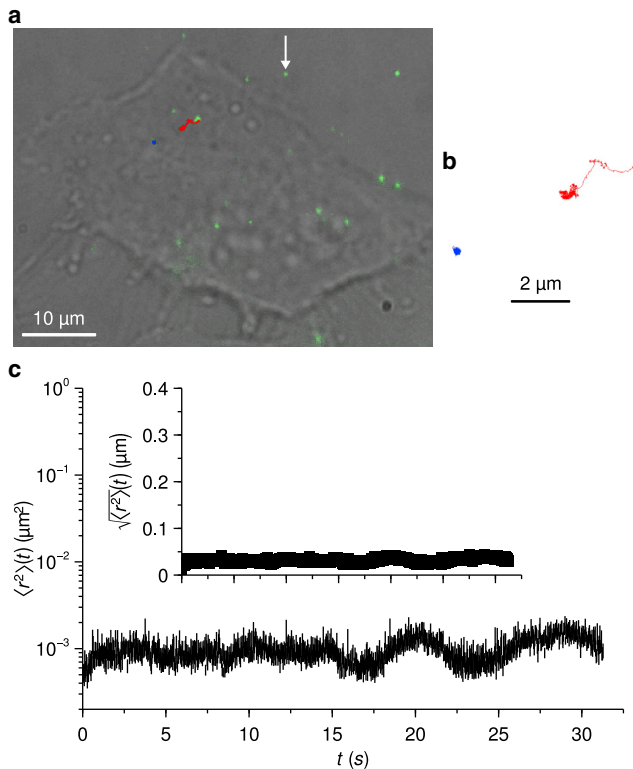
FIGURE 1 Experimental background. (*a*) Example image of a cell with beads. (*Greyscale*) Brightfield image showing the contour of the cell. (*Green*) Fluorescence image showing beads both inside the cell and (*arrow*) outside the cell. For this figure, brightness and contrast have been adjusted (uniformly over the image) to improve visibility; all image analysis was, however, performed on the original data. (*Blue* and *red lines*) Trajectories that two of the beads follow in the subsequent images of the "movie." (*b*) Zoom-in of the two trajectories shown in (*a*). One of the trajectories (*blue*) remains essentially stationary, whereas the other (*red*) moves much further. (*c*) Displacements of beads adsorbed to the glass outside the cell as a control. (*Main*) Mean-square displacement as a function of time. Note the ordinate log scale. (*Inset*) Root mean-square displacement as a function of time. Note the ordinate linear scale. In both cases, the ordinate axes have been chosen such that they are relevant for comparison with later figures (Figs. 2 *a*, 4, 5 *a*, S5, and S6, respectively). The results suggest that the beads can be followed with a precision of around $\sqrt{10^{-3}\ \mu m^2} \approx 0.03$ μm. To see this figure in color, go online.

for a different reason is not possible to tell. In contrast, the other bead (Fig. 1, *a* and *b*, *red*) moves longer, far farther than the typical radius of a lysosome (~0.2 μm). It also exhibits clear signs of motor-protein-driven transport with two stretches during which it moves almost in a straight line. In addition, the bead also spent some time "rattling around." These two examples represent the type of motion we observed in general, that is, a mixture of stalled motion, local rattling, and (semi)-unidirectional transport. Previous work has studied intracellular motion by analyzing the motion within a limited time window and categorizing it as either active or passive and thereby identifying stretches of active and passive transport, respectively (6,49). We attempted to do the same but did not find a good separation

of these two motion states at the timescales we investigated and with the time resolution we had (Fig. S2). Consequently, we continued by analyzing the motion without such a decomposition.

As a control, we tracked beads adsorbed to the glass next to cells (cf. the bead indicated by an arrow in Fig. 1 *a*; (8)), which should not move considerably. Fig. 1 *c* shows the mean-square displacement of such glass-adsorbed beads. We observe that the (tracked) positions of the beads fluctuate somewhat, as expected because of an imperfect identification of their position. However, the fluctuation in position is small, corresponding to a distance of the order of $\sqrt{10^{-3}\ \mu m^2} \approx 0.03\ \mu m$.

We next evaluated the mean-square displacement, first over an individual trajectory in which the averaging procedure is performed over time points separated by the same time (same lag time), τ. Fig. 2 *a* (*gray*) shows some examples, displaying the mean-square displacement for 20 randomly selected trajectories (Fig. S3 shows the same trajectories individually for clarity). We subsequently averaged these over all (not just the 20 exemplary) trajectories, that is, performed an ensemble average. Fig. 2 *a* (*black*) shows the results, revealing a smooth curve, suggesting that we have sampled enough trajectories to represent the average motion at the presented timescales (<15 s). The overall qualitative behavior is one of an initial plateau for times shorter than ~0.1 s, in which the mean-square displacement is relatively constant or increases very slowly with time. The origin of this plateau remains an open question. Certainly, the finite precision with which we are able to localize the beads (cf. Fig. 1 *c*) will give rise to a plateau (50–52) but so will fluctuations in the actual position (8,52,53). Conceivably, the plateau could also represent the bead moving within the enclosing structure (most of them lysosomes). However, confined diffusion is expected to plateau at a distance of the order of the size of the confining volume (54). A plateau at $3 \times 10^{-3}\ \mu m^2$ (Fig. 2 *a*) then corresponds to a radius of 55 nm (see Supporting materials and methods for more details), which is much smaller than the typical lysosome radius of 0.2 μm (48).

After the plateau is a transition period in which the mean-square displacement starts increasing more rapidly. Finally, for timescales larger than ~1 s, the mean-square displacement grows as a power law in time (note the log-log-scale in Fig. 2 *a*). It is perhaps worthwhile to compare these results with what would be expected for Brownian motion in an aqueous environment. An object of radius 0.2 μm, the typical size of a lysosome (48), would have moved $2 \times 10^{-1}\ \mu m^2$ at the shortest timescale shown in Fig. 2 *a* (see Supporting materials and methods for details). Thus, the intracellular motion we observe is far slower, underscoring the completely different nature of the cell interior.

It is to be recalled that pure Brownian motion exhibits a mean-square displacement that grows linearly with time, that is, a power law with an exponent of 1 ($\alpha = 1$ in
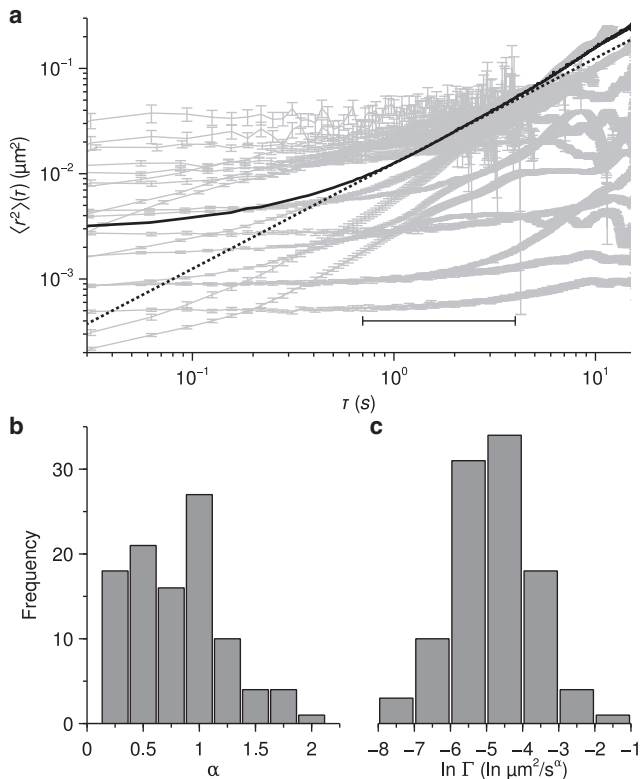
a

b   c

FIGURE 2 The motion is heterogeneous. (*a*) Mean-square displacements. (*Gray*) Lag-time-averaged mean-square displacement of 20 randomly chosen trajectories. Error bars indicate standard error of the mean. Fig. S3 shows the results individually for clarity. (*Black*) Lag-time- and ensemble-averaged mean-square displacements (over all trajectories, not just the 20 randomly chosen ones). Error bars indicate standard error of the mean over trajectories, though most of them are too small to be visible. (*Dotted line*) Straight line with a slope of unity, characteristic of Brownian motion. (*Interval*) Time period in which the mean-square displacements were fitted to a power law (Eq. 1). (*b* and *c*) Distribution of the exponent, α, and the prefactor, Γ, of fits of a power law (Eq. 1) to the mean-square displacements in the interval 0.7–4 s (indicated in *a*). Note that all trajectories were used not just the 20 random examples. Overall, the results show that the motion is heterogeneous and that for timescales larger than ∼1 s, the mean-square displacement grows as a power law with an exponent close to unity.

Eq. 1). The converse is not necessarily true, that is, a power law exponent of 1 can also be observed when motion is more complex than pure Brownian motion (19,55). Exponents different from unity are called anomalous and are further divided into subdiffusive, in which the mean-square displacement grows slower than time ($\alpha < 1$), and superdiffusive, in which the mean-square displacement grows more rapidly ($\alpha > 1$). Moreover, if an object moves with a constant velocity, then we expect a mean-square displacement that grows with time squared ($\alpha = 2$), referred to as ballistic. This is relevant for motion inside the cell because we expect this behavior if an object is pulled by motor proteins at constant speed (6,56).

We clearly do not have a single type of behavior but one that changes with timescale (Fig. 2 *a*). However, for time-

scales larger than ∼1 s, we do observe a power law increase of the mean-square displacement with time with an exponent that is somewhat higher than unity (cf. the *dotted line* in Fig. 2 *a*), though this is a minor effect. Regardless, even at second timescales, the mean-square displacement is far from ballistic ($\propto \tau^2$) in contrast to what would be expected for (pure) motor-protein-driven intracellular transport (6,56).

The observed behavior is very similar to the motion of 100–500-nm-sized PEGylated polystyrene beads free in the cytosol of A7 human melanoma cells reported previously (8). Indeed, although the initial plateau occurs at a different value and the exponent we find is possibly slightly higher, the mean-square displacement otherwise appears almost quantitatively similar. This may be considered somewhat surprising because the particles followed in that report are free in the cytosol, whereas the particles we study are enclosed in membrane-surrounded structures and (also) move by motor proteins. The same work also reports the motion of vesicles and protein complexes inside cells, which we would expect to be a closer analogy to our system. Curiously, though, that motion appears less similar, though a reason could simply be that their experiments were performed at too long a timescale to capture the short timescale plateau (8). Additionally, the motion of endogenous intracellular particles in *Acanthamoeba castellanii* (57,58), acetylcholine receptors (59) and ganglioside GM1 glycosphingolipids (60) in cell membranes of muscle cells cultured from clawed frog (*Xenopus*) embryos and melanosomes in African clawed frog (*Xenopus laevis*) melanophores (61) also appears to be rather similar to our results. However, in the latter case, we base that contention on a comparison with individual trajectories rather than the ensemble average. Finally, membrane-embedded integrin receptors of human airway smooth muscle cells also appear to exhibit a similar type of motion but only under cell-energy-depleted conditions (20). Aside from these literature observations on biological systems, we note that the mean-square displacement is qualitatively similar to that observed in colloidal glasses. That is, when a colloidal glass is close to but not at the glass transition, the mean-square displacement also exhibits a plateau at short timescales and a power law increase with an exponent close to unity at longer timescales (14).

At the level of individual trajectories, Fig. 2 *b* (*gray*) shows the mean-square displacement for 20 randomly selected trajectories. The majority of them share the qualitative behavior of the equivalent ensemble average (*black*). That is, many of them exhibit an initial plateau for timescales shorter than 0.1–1 s in which the mean-square displacement is relatively constant (or increases very slowly), followed by a more rapid rise as a function of time.

Despite these similarities, the motion appears highly heterogeneous in nature, with the 20 randomly selected trajectories looking very different from each other.

Heterogeneous motion is a common observation in biological systems, including for lipid granules in yeast (*Schizosaccharomyces pombe*) (4,62), messenger RNA (mRNA) molecules in *E. coli* (9,63), integrin receptors on the membrane of human airway smooth muscle cells (64), endogenous particles in *Amoeba proteus* (65), endogenous granules, and 200-nm carboxylated polystyrene particles free in the cytosol of Hmec-1 human microvascular endothelial cells (66), melanosomes in African clawed frog (*X. laevis*) melanophores (61), chains of endosomes in PC3 human prostate cancer cells (67), Kv2.1 potassium channels in cell membranes of human embryonic kidney cells (68), insulin granules in MIN6 mouse cells (7), PEGylated polystyrene beads free in the cytosol of A7 human melanoma cells (8), endogenous intracellular particles in *A. castellanii* (57,58), and mRNA molecules in *S. cerevisiae* (63).

As a measure of the heterogeneity of the motion, we fitted a power law (Eq. 1) to the mean-square displacement of each trajectory. We chose to do this in the interval 0.7–4 s (as indicated in Fig. 2 *a*), which is after the initial plateau (Fig. 2 *a*). Fig. 2, *b* and *c* shows the distribution of the exponent, α, and the prefactor, Γ, obtained from such power law fits. Fig. 2 *b* shows that the motion covers a wide range, from subdiffusive ($\alpha < 1$) through exponents close to unity ($\alpha \sim 1$) to superdiffusive ($\alpha > 1$), though only one trajectory appears (purely) ballistic ($\alpha = 2$) at these timescales. Fig. 2 *c* shows a large spread between the trajectories also for the prefactor, Γ. Overall, the motion is indeed heterogeneous.

We next aimed at elucidating whether the motion is ergodic. In general, an ergodic system is one in which ensemble and time averages are equal. In this context, this implies whether averages over (sufficiently many) trajectories equal an average over (a sufficiently long) time for an individual trajectory. Pure Brownian motion is ergodic, that is, the two averages agree. However, many models of random motion break ergodicity (39,40). It must be emphasized that the source of the lack of ergodicity is not the separation of phase space into mutually inaccessible domains (as in, e.g., an Ising magnet below the critical temperature) and to distinguish one refers to the ergodicity breaking as weak. (Weakly) nonergodic behavior is typical of, but not exclusive to, glassy dynamics in which the concept was first introduced (32).

To quantify the degree of ergodicity breaking, we used a parameter previously introduced for this purpose (38–40) that gives a numerical measure of the degree of ergodicity breaking as a function of lag time, τ. This parameter is defined as an infinite time limit (see Eq. 2 in Materials and methods) that we obviously cannot observe experimentally; instead, we evaluated the corresponding time-dependent quantity, $EB_t(\tau)$. Fig. 3 *a* shows this time-dependent quantity for three different lag times (with other lag times reported in Fig. S4). For the two shorter lag times, we observe a clear attainment of a plateau, and also for the longer lag time, the value appears to have stabilized. For
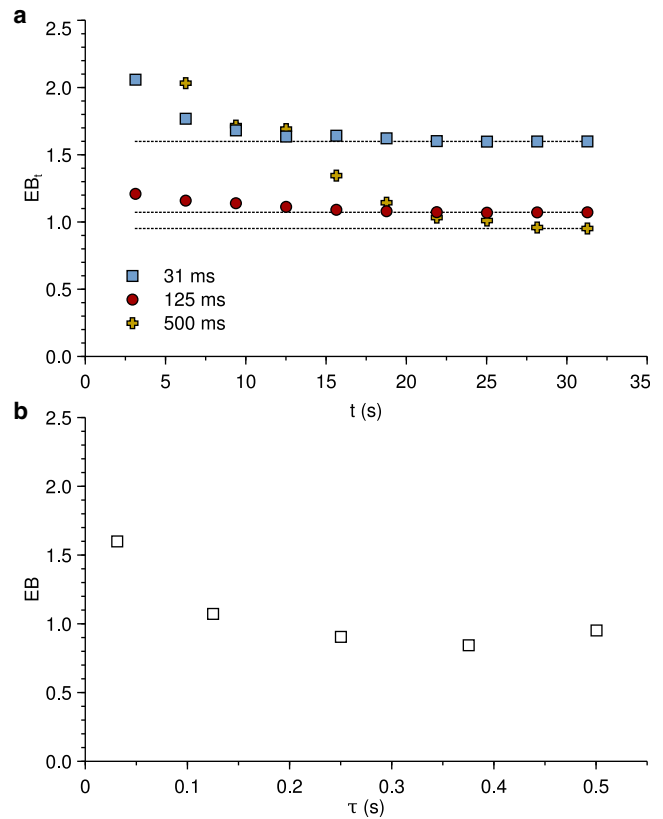

FIGURE 3 The motion is not ergodic. (*a*) (*Data points*) Quantity that tends to a parameter that measures the degree of ergodicity breaking in the infinite time limit evaluated for the three different lag times indicated in the figure. (*Dotted lines*) Final value as a guide to the eye for evaluating the convergence. (*b*) Ergodicity breaking parameter as a function of lag time, τ. The ergodicity breaking parameter was estimated as the final value from results such as those shown in (*a*); the lag times not shown in (*a*) are reported in Fig. S4. The ergodicity breaking parameter is 0 for an ergodic process, so the results show that the motion is nonergodic. To see this figure in color, go online.

even longer lag times, the plateaus become less certain (Fig. S4). Estimating the ergodicity breaking parameter as the value obtained at the longest time investigated, Fig. 3 *b* thus shows the ergodicity breaking parameter as a function of lag time. For an ergodic process, the ergodicity breaking parameter is 0, independently of lag time (7); clearly our observations are distinct from 0, showing that the motion is nonergodic.

Nonergodic behavior was previously shown for the motion of lipid granules in *S. pombe* (62), Kv2.1 potassium channels in cell membranes of human embryonic kidney cells (68), insulin granules in MIN6 mouse cells (7), and dendritic-cell-specific intercellular adhesion molecule three-grabbing nonintegrin receptors in cell membranes of Chinese hamster ovary cells (69). In contrast, 150-nm particles free in the cytosol of slime mold *Dictyostelium discoideum* cells were shown to move in an ergodic fashion using the same ergodicity breaking parameter (70).

To characterize the motion in more detail, we focused on relatively short (submicron) length scales but ones that nevertheless extend beyond the typical radius of a lysosome (0.2 μm) to ensure that the motion does not represent confinement. We started by assessing the displacement distribution. Especially in the glass literature, the displacement distribution also goes under the name of the self-part of the van Hove function, $G_s(\Delta r; \tau)$ (16), and represents the probability that a particle has moved a distance, Δr, from its starting point at time, τ. We evaluated the displacement distribution in two dimensions as a function of radial distance and present our results excluding the $2\pi\Delta r$ factor that stems from the two-dimensional geometry. As is well-known, for a diffusive process, the displacement distribution is a Gaussian. Fig. 4 a, however, clearly shows that our results are not well described by a Gaussian; rather than decaying exponentially with Δr^2, the displacement distribution decays slower, exponentially with Δr (note the semi-log-scale in Fig. 4 a).

Non-Gaussian displacement distributions have been observed in a range of biological systems, including insulin granules in MIN6 mouse cells (7), GFP-μNS particles in *E. coli* (10) and *S. cerevisiae* (11), beads on the membrane of human airway smooth muscle cells (20), beads in F-actin networks (19), 150-nm particles free in the cytosol of slime mold *D. discoideum* cells (70), mRNA particles in *S. cerevisiae* (63,75) and *E. coli* (63,76), Kv2.1 potassium channels in cell membranes of human embryonic kidney cells (68), acetylcholine receptors (59) and ganglioside GM1 glycosphingolipids (60) in cell membranes of muscle cells cultured from clawed frog (*Xenopus*) embryos, reconstituted actin networks containing myosin (77,78), and quantum dots injected into fibrosarcoma and fibroblast cells (79). Additionally, though not exclusive to glasses, they are a hallmark of glassy dynamics.

To explore the analogy with glassy systems quantitatively, we adopted the model introduced by Chaudhuri et al. (41,42). They considered the displacement distributions from several different glassy systems studied experimentally, namely a dense hard-sphere colloidal system (14), a binary granular system (71), and a dense attracting colloidal system (42). Similarly, they studied the displacement distributions from simulations of a binary Lennard-Jones particle mixture (72) and ones mimicking a silica melt (73,74). All of these systems exhibit very similar displacement distributions, thus suggesting a universal nature of the displacement distribution of glassy systems (41,42). Chaudhuri et al. (41,42) were, furthermore, able to describe these displacement distributions quantitatively in terms of a simple model in which at short timescales, objects just "rattle around" locally, unable to move far, whereas at longer timescales, objects take more extended jumps. Their model also includes a different waiting time before the object makes the first jump, compared with how long the object waits before taking a subsequent jump. For this type of motion, the mean-square displacement (Fig. 2 a) takes a very different interpretation. Thus, in the Chaudhuri et al. (41,42) model, objects are either stationary or moving, and their average thus does not represent either of them well but rather more reflects the transition from stationary to moving. Thus, although for pure Brownian motion the mean-square displacement provides a useful measure of the average motion, it is less useful as a measure of the average distance traveled in the Chaudhuri et al. (41,42) model.

To use the Chaudhuri et al. (41,42) model on our data, we solved it in two dimensions (see Supporting materials and methods for details). The resulting expression for the displacement distribution depends on time and has four free parameters. We fitted this model to the experimental displacement distributions for different times simultaneously (i.e., a "global fit" with four free parameters in
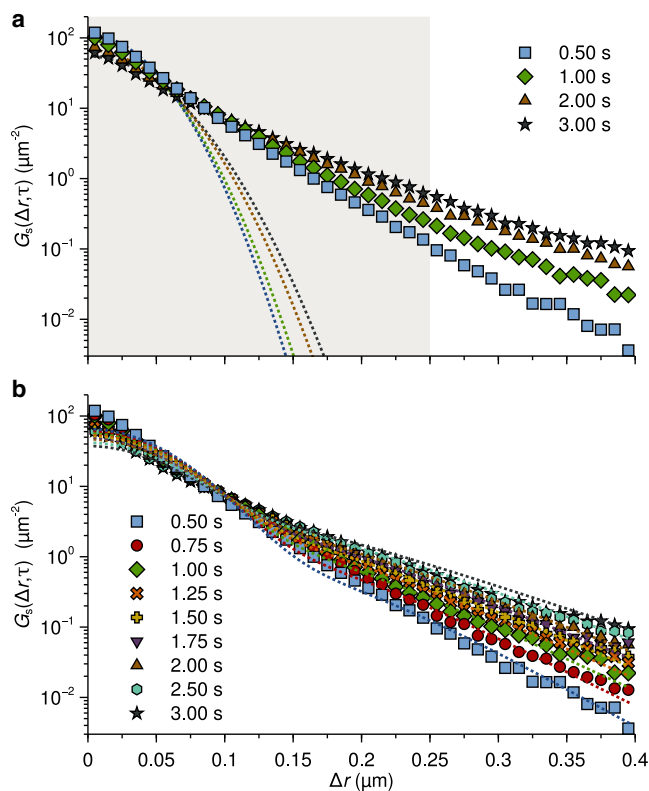

FIGURE 4 The displacement distributions are not Gaussian but can be described by a model for glassy dynamics. (*a*) (*Data points*) Displacement distributions measured experimentally for a few exemplar lag times, τ. (*Dotted lines*) Fits of a Gaussian (Eq. 3) to the data for $\Delta r < 0.25$ μm (*shaded region*). (*b*) (*Data points*) Several other displacement distributions. (*Dotted lines*) Fits of the Chaudhuri et al. model (41,42) (see Supporting materials and methods) to the data (for the whole interval shown) with the four parameters of the model demanded to be the same for all curves. The curves are shown individually in Fig. S5. Note the ordinate log scale in both panels. The Chaudhuri et al. model has been shown to describe the dynamics in a range of glassy systems (14,41,42,71–74); the good fit of this model to the data thus suggests that our system shares features with glassy systems. To see this figure in color, go online.

total). We reiterate that we evaluated the displacement distribution for distances longer than the typical radius of the lysosomes (0.2 μm), so we expect that the motion we capture is motion of the containing structure, rather than the bead being confined within it. Fig. 4 b shows that this model, indeed, provides a good description of the data, suggesting a quantitative connection between our system and a range of glassy systems.

We note that the majority of systems tested by Chaudhuri et al. (41,42) contain a prominent short-distance Gaussian in the displacement distribution, something that is less obvious in our data (Fig. 4, a and b). However, at longer timescales and/or further away from the glass transition, we expect this Gaussian to become less prominent and, indeed, that appears to be the case also for the systems tested by Chaudhuri et al. where applicable (42,71). Within the framework of glassy dynamics, we may thus interpret the lack of a prominent Gaussian in our data (Fig. 4, a and b) as a reflection either of a limited time resolution (roughly 31 ms) or, possibly, as the system being at some distance from the glass transition. We stress that the last statement should be read in a loose sense because we are considering glassy dynamics as a potential analogy rather than the cell having undergone a glass transition in a literal sense.

We next attempted at extracting more information by fitting a purely exponentially decaying function, with a lag-time-dependent decay length, $\lambda(\tau)$, to the data (see Eq. 4 in Materials and methods). Some caution may be warranted here because it has been argued in the context of the Chaudhuri et al. model that there is no particular significance to $\lambda(\tau)$ (42). Still, we do not necessarily expect glassy dynamics to describe the motion at all time and length scales, so we present the following results as a purely empirical observation. To account for the nonexponential nature at short distances, we performed the fit only after $\Delta r = 0.1$. Fig. 5 a shows that such fits describe the data well for a range of different times. Moreover, we can thereby follow the time evolution of the decay length $\lambda(\tau)$. It turns out that the decay length grows, to a good approximation, as a power law in (lag) time, namely as $\tau^{0.27}$ (Fig. 5 b). Indeed, if we normalize space in this way, we find an acceptable collapse, given the highly complex system we are investigating, of all displacement distributions to a single master curve (Fig. 5 c).

For a purely diffusive process, we also expect a collapse of the curves if we normalize space appropriately, in that case with $\tau^{1/2}$. Nevertheless, a collapse of the displacement distributions after normalizing space by $\tau^{1/2}$ is more general than pure diffusion. Thus, a range of systems, including beads (19) and liposomes (55) in F-actin networks, as well as tracer particles in larger hard-sphere colloidal suspensions (80), exhibit non-Gaussian displacement distributions, which nevertheless collapse when space is normalized by $\tau^{1/2}$. We should stress though that the exponent ~ 0.27 we find is clearly distinct from 1/2. To our knowledge, a similar exponent has not been reported in biological systems.

We continued by evaluating another hallmark of glassy dynamics, namely decoupling of persistence and exchange times (33,34). In this context, the persistence time is how long it takes a particle to move a certain distance for the first time, whereas the exchange time is how long it takes the particle to move the same distance again (34). Generally speaking, for most systems, including Brownian motion, the persistence and exchange times have the same distribution. In glassy systems, however, the distributions are different, that is, the persistence and exchange times are decoupled.

To calculate the persistence and exchange times from our data, we had to make a choice of the distance to consider. We chose 0.2 μm, which corresponds to the lysosome radius (48), but we also report the results for a few other choices in Fig. S7. In all cases, we chose distances clearly above the localization precision for beads adsorbed to glass (0.03 μm; Fig. 1 c). For a distance of 0.2 μm, Fig. 6 shows that the exchange time distribution is monotonically decreasing, whereas the persistence time distribution exhibits some sort of a plateau before decaying. Importantly, the clear difference between the two distributions is evidence of a decoupling between the persistence and exchange times. This conclusion is independent of the distance we choose within moderate variations (Fig. S7).

Because of the finite time resolution (around 31 ms), there is the possibility that a bead moves the 0.2 μm but then moves back again without us registering it as a larger than 0.2-μm movement. This would imply that some of the events we consider to be persistence events are actually exchange events. However, a movement of 0.2 μm in 31 ms demands a speed of 0.2 μm/31 ms $\approx$ 6.5 μm/s. Such speeds are possible for motor-protein-driven transport but are toward the upper end of the speed distribution one observes when organelles move in effectively one-dimensional cellular protrusions (56). We thus expect the likelihood of this happening to be fairly low. Furthermore, when we consider larger distances (0.25–0.35 μm), the probability of us not identifying a persistence event decreases because the speed with which the bead has to move increases (8.1– 11 μm/s). Nevertheless, the difference between the persistence and exchange time distributions remains (Fig. S7).

The persistence and exchange times have been evaluated for a few other biologically relevant systems. Thus, for the motion of beads in F-actin networks, there was no evidence for a decoupling of the exchange and persistence times (19), whereas for the motion of insulin granules in MIN6 mouse cells, a clear decoupling has been observed (7).

CONCLUSIONS

Our motivation for this work was the notion that glassy dynamics provides a useful conceptual basis for how objects move inside the cell. Previous studies have tested this idea for cytosolic motion in microorganisms, such as bacteria
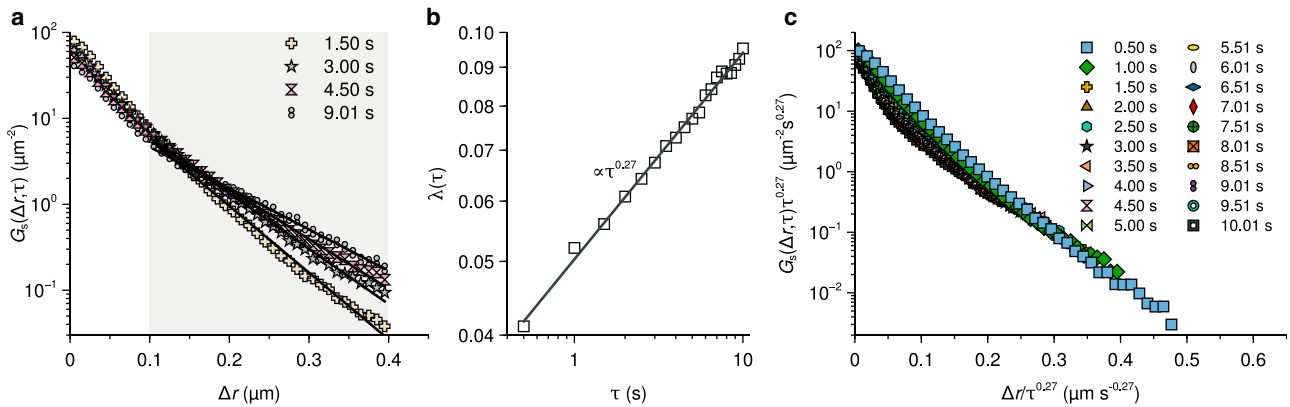
FIGURE 5 The displacement distribution decays exponentially with a decay length that grows as a power law in time. (*a*) (*Data points*) Displacement distributions for a few exemplar lag times, τ. Other examples are shown in Fig. S6. (*Lines*) Fits of an exponentially decaying function in the interval 0.10 μm < Δr < 0.40 μm (*shaded region*). (*b*) Decay length ($\lambda(\tau)$ in Eq. 4) extracted from fits such as those shown in (*a*) as a function of lag time, τ. Note that only a few of the fits that underlie (*b*) are shown in (*a*) to make that panel legible. (*Solid line*) Power law fit to the data, giving an exponent 0.27. Note the log-log-scale. (*c*) Collapse of all curves onto a universal master curve after taking into account the power law growth of the exponential decay length. Overall, the results suggest that an exponentially decaying displacement distribution shows a reasonable description of the data for intermediate length scales (0.10 μm < Δr < 0.40 μm). To see this figure in color, go online.

(*E. coli*) (10) and yeast (*S. cerevisiae*) (11). Here, we posed the question whether glass-like motion is also observed in human cells and for objects that can move by motor proteins. With that in mind, we investigated several features typical of, though not exclusive to, glassy dynamics. As a cell system, we chose to use a common human cell type, thus allowing our observations both to be informed by and to inform on fundamental studies in cell biology. As probes, we used nanosized beads because of their ease of use and because they (predominantly) localize to lysosomes and thus allow following their motion.

Our results show that the motion of the beads is heterogeneous (Fig. 2) and nonergodic (Fig. 3), both characteristics shared by glassy systems. Furthermore, focusing on relatively short length scales, our data are well described by a model that has been used to demonstrate the universality of the displacement distribution for a range of glassy systems (Fig. 4). Finally, the exchange and persistence times are decoupled (Fig. 6), another hallmark of glassy dynamics. All in all, the motion we observe thus shares several features typical of glassy systems.

We should stress, though, that we view the observation of glassy motion as a useful analogy. That is, we do not claim that the cell actually is in a glassy state in the sense of a physical glass (16); rather, we claim that the motion we observe exhibits similar features to that in the glassy state. Related to that, we remain agnostic on the mechanism underlying the observed motion. Though the mechanism behind the motion in a glass is itself debated, it is often described in terms of objects blocking each other from moving for extended periods of time, only infrequently opening up to allow large-scale motion (41), something that is also associated with the idea of dynamical heterogeneity (81). This is certainly a possibility also inside the crowded cell

interior, but even so, it will be shaped by the heterogeneity of the objects that can block each other. That is, in physical glasses, one typically considers systems consisting of a single (12–14,16) or at most a few (15) types of objects and typically with a low variability in size. In the cell, various types of organelles, vesicles, and complexes can block each other, not only one type. Added to the complexity of such interactions is the fact that the objects will vary in
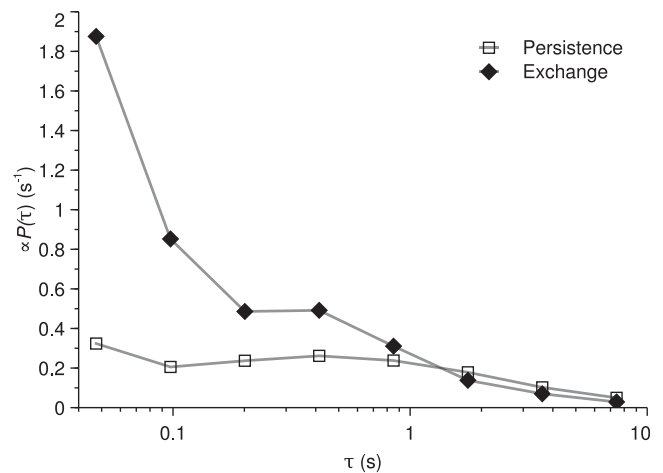

FIGURE 6 Decoupling of persistence and exchange times. The distribution of times it takes to move a distance of 0.2 μm for the first time since the start of observation (persistence time) together with the times it takes to subsequently move the same distance a second time (exchange time). The results for a few other distances are shown in Fig. S7. For technical reasons, the distribution was not sampled beyond 10 s (see Materials and methods), so the results are just proportional to the actual distribution. However, given that the distributions have decayed substantially, the major statistical weight should have been sampled. The fact that the persistence and exchange time distributions are different (decoupled) is another characteristic of glassy dynamics that is evidently shared by our system.

size and shape, even for the same type of organelle. Similarly, the cytoskeleton will likely play a large role in impeding the motion (8), and this network is not spatially heterogeneous.

Aside from blocking, there are also other, not mutually exclusive, possible mechanisms. For example, the membrane-surrounded compartment that holds the bead could detach from the cytoskeleton, and this could be the underlying reason the beads often remain stationary. Similarly, motor proteins could be pulling the object in different directions, thereby causing a stall until one direction triumphs in such a "tug of war" (56,82). One could even envisage a local cell energy depletion explaining a temporary lack of motion before the arrival of cell energy (ATP). It is readily imagined that stalled (or possibly diffusive) motion stemming from such molecular mechanisms, when combined with stretches of driven motion, could give rise to the observations we make. For example, the non-Gaussian character of the displacement distribution would then be a combination of short (or nonexistent) steps due to stalling, together with longer steps associated with stretches of driven transport. Similarly, the decoupling of persistence and exchange times could be interpreted as the object having a tendency to keep moving actively once it has started. Naturally, for this possibility to be true, our data place certain demands on the probability to start moving, the velocity distribution, the propensity to keep moving actively once started, etc. We know of no mechanistic model that has already demonstrated these outcomes, but this could be an interesting pursuit.

Regardless of the underlying mechanisms potentially being different, linking the motion of objects that can move actively via motor proteins inside the cell to the problem of the glass transition, itself currently being clarified (83), may turn out to be a far-reaching and fruitful endeavor. Indeed, this has been the case for the motion of cells themselves, in which an analogy with glassy dynamics has prompted a number of interesting results on the motion in dense cell populations (84–87). It will be relevant to test our conclusions also on other organelles and cell systems, and establish their (potential) generality. It would, furthermore, be important to investigate the motion at longer length scales (88), beyond the submicron lengths we focus on here, and relate that to cellular trafficking processes. This is important because a range of applications hinge upon an understanding of how cells traffic materials. Thus, nanosized drug delivery vehicles often also follow the endolysosomal pathway (89–92), and the slow kinetics implied by glass-like dynamics could have real implications on the efficiency of drug delivery. Such examples highlight the significance of understanding the motion inside cells and the processes that depend upon it.

SUPPORTING MATERIAL

Supporting material can be found online at https://doi.org/10.1016/j.bpj.2021.04.011.

AUTHOR CONTRIBUTIONS

ACKNOWLEDGMENTS

SUPPORTING CITATIONS

References (93–95) appear in the Supporting Material.

REFERENCES

1. Frey, E., and K. Kroy. 2005. Brownian motion: a paradigm of soft matter and biological physics. *Ann. Phys.* 14:20–50.

2. Höfling, F., and T. Franosch. 2013. Anomalous transport in the crowded world of biological cells. *Rep. Prog. Phys.* 76:046602.

3. Caspi, A., R. Granek, and M. Elbaum. 2000. Enhanced diffusion in active intracellular transport. *Phys. Rev. Lett.* 85:5655–5658.

4. Tolić-Nørrelykke, I. M., E.-L. Munteanu, …, K. Berg-Sørensen. 2004. Anomalous diffusion in living yeast cells. *Phys. Rev. Lett.* 93:078102.

5. Weihs, D., T. G. Mason, and M. A. Teitell. 2007. Effects of cytoskeletal disruption on transport, structure, and rheology within mammalian cells. *Phys Fluids (1994)*. 19:103102.

6. Arcizet, D., B. Meier, …, D. Heinrich. 2008. Temporal analysis of active and passive transport in living cells. *Phys. Rev. Lett.* 101:248103.

7. Tabei, S. M. A., S. Burov, …, N. F. Scherer. 2013. Intracellular transport of insulin granules is a subordinated random walk. *Proc. Natl. Acad. Sci. USA.* 110:4911–4916.

8. Guo, M., A. J. Ehrlicher, …, D. A. Weitz. 2014. Probing the stochastic, motor-driven properties of the cytoplasm using force spectrum microscopy. *Cell.* 158:822–832.

9. Golding, I., and E. C. Cox. 2006. Physical nature of bacterial cytoplasm. *Phys. Rev. Lett.* 96:098102.

10. Parry, B. R., I. V. Surovtsev, …, C. Jacobs-Wagner. 2014. The bacterial cytoplasm has glass-like properties and is fluidized by metabolic activity. *Cell.* 156:183–194.

11. Munder, M. C., D. Midtvedt, …, S. Alberti. 2016. A pH-driven transition of the cytoplasm from a fluid- to a solid-like state promotes entry into dormancy. *eLife.* 5:e09347.

12. van Blaaderen, A., and P. Wiltzius. 1995. Real-space structure of colloidal hard-sphere glasses. *Science.* 270:1177–1179.

13. Kegel, W. K., and A. van Blaaderen. 2000. Direct observation of dynamical heterogeneities in colloidal hard-sphere suspensions. *Science.* 287:290–293.

14. Weeks, E. R., J. C. Crocker, …, D. A. Weitz. 2000. Three-dimensional direct imaging of structural relaxation near the colloidal glass transition. *Science.* 287:627–631.

15. Sentjabrskaja, T., E. Zaccarelli, …, M. Laurati. 2016. Anomalous dynamics of intruders in a crowded environment of mobile obstacles. *Nat. Commun.* 7:11133.

16. Binder, K., and W. Kob. 2005. Glassy Materials and Disordered Solids: An Introduction to Their Statistical Mechanics. World Scientific, Singapore.

17. Dawson, K. A. 2002. The glass paradigm for colloidal glasses, gels, and other arrested states driven by attractive interactions. *Curr. Opin. Colloid Interface Sci.* 7:218–227.

18. Janmey, P. A., and F. C. MacKintosh. 2014. Cytoplasmic transport: bacteria turn to glass unless kicked. *Curr. Biol.* 24:R226–R228.

19. Wang, B., S. M. Anthony, …, S. Granick. 2009. Anomalous yet Brownian. *Proc. Natl. Acad. Sci. USA.* 106:15160–15164.

20. Bursac, P., G. Lenormand, …, J. J. Fredberg. 2005. Cytoskeletal remodelling and slow dynamics in the living cell. *Nat. Mater.* 4:557–561.

21. Joyner, R. P., J. H. Tang, …, K. Weis. 2016. A glucose-starvation response regulates the diffusion of macromolecules. *eLife.* 5:e09376.

22. Mittasch, M., P. Gross, …, M. Kreysing. 2018. Non-invasive perturbations of intracellular flow reveal physical principles of cell organization. *Nat. Cell Biol.* 20:344–351.

23. Mignot, T., and J. W. Shaevitz. 2008. Active and passive mechanisms of intracellular transport and localization in bacteria. *Curr. Opin. Microbiol.* 11:580–585.

24. Rejman, J., V. Oberle, …, D. Hoekstra. 2004. Size-dependent internalization of particles via the pathways of clathrin- and caveolae-mediated endocytosis. *Biochem. J.* 377:159–169.

25. Salvati, A., C. Åberg, …, K. A. Dawson. 2011. Experimental and theoretical comparison of intracellular import of polymeric nanoparticles and small molecules: toward models of uptake kinetics. *Nanomedicine (Lond.).* 7:818–826.

26. Sandin, P., L. W. Fitzpatrick, …, K. A. Dawson. 2012. High-speed imaging of Rab family small GTPases reveals rare events in nanoparticle trafficking in living cells. *ACS Nano.* 6:1513–1521.

27. Varela, J. A., C. Åberg, …, K. A. Dawson. 2015. Trajectory-based co-localization measures for nanoparticle-cell interaction studies. *Small.* 11:2026–2031.

28. Åberg, C., J. A. Varela, …, K. A. Dawson. 2016. Spatial and structural metrics for living cells inspired by statistical mechanics. *Sci. Rep.* 6:34457.

29. Lesniak, A., A. Salvati, …, C. Åberg. 2013. Nanoparticle adhesion to the cell membrane and its effect on nanoparticle uptake efficiency. *J. Am. Chem. Soc.* 135:1438–1444.

30. Kim, J. A., C. Åberg, …, K. A. Dawson. 2011. Role of cell cycle on the cellular uptake and dilution of nanoparticles in a cell population. *Nat. Nanotechnol.* 7:62–68.

31. Bramini, M., D. Ye, …, K. A. Dawson. 2014. Imaging approach to mechanistic study of nanoparticle interactions with the blood-brain barrier. *ACS Nano.* 8:4304–4312.

32. Bouchaud, J.-P. 1992. Weak ergodicity breaking and aging in disordered systems. *J. Phys. I France.* 2:1705–1713.

33. Jung, Y., J. P. Garrahan, and D. Chandler. 2004. Excitation lines and the breakdown of Stokes-Einstein relations in supercooled liquids. *Phys. Rev. E Stat. Nonlin. Soft Matter Phys.* 69:061205.

34. Hedges, L. O., L. Maibaum, …, J. P. Garrahan. 2007. Decoupling of exchange and persistence times in atomistic models of glass formers. *J. Chem. Phys.* 127:211101.

35. Tinevez, J.-Y., N. Perry, …, K. W. Eliceiri. 2017. TrackMate: an open and extensible platform for single-particle tracking. *Methods.* 115:80–90.

36. Schindelin, J., I. Arganda-Carreras, …, A. Cardona. 2012. Fiji: an open-source platform for biological-image analysis. *Nat. Methods.* 9:676–682.

37. Schneider, C. A., W. S. Rasband, and K. W. Eliceiri. 2012. NIH Image to ImageJ: 25 years of image analysis. *Nat. Methods.* 9:671–675.

38. He, Y., S. Burov, …, E. Barkai. 2008. Random time-scale invariant diffusion and transport coefficients. *Phys. Rev. Lett.* 101:058101.

39. Burov, S., J.-H. Jeon, …, E. Barkai. 2011. Single particle tracking in systems showing anomalous diffusion: the role of weak ergodicity breaking. *Phys. Chem. Chem. Phys.* 13:1800–1812.

40. Metzler, R., J.-H. Jeon, …, E. Barkai. 2014. Anomalous diffusion models and their properties: non-stationarity, non-ergodicity, and ageing at the centenary of single particle tracking. *Phys. Chem. Chem. Phys.* 16:24128–24164.

41. Chaudhuri, P., L. Berthier, and W. Kob. 2007. Universal nature of particle displacements close to glass and jamming transitions. *Phys. Rev. Lett.* 99:060604.

42. Chaudhuri, P., Y. Gao, …, W. Kob. 2008. A random walk description of the heterogeneous glassy dynamics of attracting colloids. *J. Phys. Condens. Matter.* 20:244126.

43. Virtanen, P., R. Gommers, …, P. van Mulbregt; SciPy 1.0 Contributors. 2020. SciPy 1.0: fundamental algorithms for scientific computing in Python. *Nat. Methods.* 17:261–272.

44. Harris, C. R., K. J. Millman, …, T. E. Oliphant. 2020. Array programming with NumPy. *Nature.* 585:357–362.

45. Iversen, T.-G., T. Skotland, and K. Sandvig. 2011. Endocytosis and intracellular transport of nanoparticles: present knowledge and need for future studies. *Nano Today.* 6:176–185.

46. Xiong, R., F. Joris, …, K. Braeckmans. 2016. Cytosolic delivery of nanolabels prevents their asymmetric inheritance and enables extended quantitative in vivo cell imaging. *Nano Lett.* 16:5975–5986.

47. Alberts, B., A. Johnson, …, P. Walter. 2008. Chapter 13. Intracellular vesicle traffic. Molecular Biology of the Cell. Garland Science, pp. 711–766.

48. Novikoff, A. B. 1961. Lysosomes and related particles. *In* The Cell. Vol. 2, Cells and their Component Parts. J. Brachet and A. E. Mirsky, eds. Academic Press, pp. 423–488.

49. Mahowald, J., D. Arcizet, and D. Heinrich. 2009. Impact of external stimuli and cell micro-architecture on intracellular transport states. *ChemPhysChem.* 10:1559–1566.

50. Thompson, R. E., D. R. Larson, and W. W. Webb. 2002. Precise nanometer localization analysis for individual fluorescent probes. *Biophys. J.* 82:2775–2783.

51. Michalet, X. 2010. Mean square displacement analysis of single-particle trajectories with localization error: Brownian motion in an isotropic medium. *Phys. Rev. E Stat. Nonlin. Soft Matter Phys.* 82:041914.

52. Song, M. S., H. C. Moon, …, H. Y. Park. 2018. Neuronal messenger ribonucleoprotein transport follows an aging Lévy walk. *Nat. Commun.* 9:344.

53. Yamada, S., D. Wirtz, and S. C. Kuo. 2000. Mechanics of living cells measured by laser tracking microrheology. *Biophys. J.* 78:1736–1747.

54. Bickel, T. 2007. A note on confined diffusion. *Phys. Stat. Mech. Its Appl.* 377:24–32.

55. Wang, B., J. Kuo, …, S. Granick. 2012. When Brownian diffusion is not Gaussian. *Nat. Mater.* 11:481–485.

56. Kural, C., H. Kim, …, P. R. Selvin. 2005. Kinesin and dynein move a peroxisome in vivo: a tug-of-war or coordinated movement? *Science.* 308:1469–1472.

57. Reverey, J. F., J.-H. Jeon, …, C. Selhuber-Unkel. 2015. Superdiffusion dominates intracellular particle motion in the supercrowded cytoplasm of pathogenic Acanthamoeba castellanii. *Sci. Rep.* 5:11690.

58. Krapf, D., N. Lukat, …, X. Xu. 2019. Spectral content of a single non-Brownian trajectory. *Phys. Rev. X.* 9:011019.

59. He, W., H. Song, …, P. Tong. 2016. Dynamic heterogeneity and non-Gaussian statistics for acetylcholine receptors on live cell membrane. *Nat. Commun.* 7:11701.

60. He, W., Y. Su, …, P. Tong. 2020. Dynamic heterogeneity and non-Gaussian statistics for ganglioside GM1s and acetylcholine receptors on live cell membrane. *Mol. Biol. Cell.* 31:1380–1391.

61. Brunstein, M., L. Bruno, …, V. Levi. 2009. Anomalous dynamics of melanosomes driven by myosin-V in *Xenopus laevis* melanophores. *Biophys. J.* 97:1548–1557.

62. Jeon, J.-H., V. Tejedor, …, R. Metzler. 2011. In vivo anomalous diffusion and weak ergodicity breaking of lipid granules. *Phys. Rev. Lett.* 106:048103.

63. Lampo, T. J., S. Stylianidou, …, A. J. Spakowitz. 2017. Cytoplasmic RNA-protein particles exhibit non-Gaussian subdiffusive behavior. *Biophys. J.* 112:532–542.

64. Bursac, P., B. Fabry, …, S. S. An. 2007. Cytoskeleton dynamics: fluctuations within the network. *Biochem. Biophys. Res. Commun.* 355:324–330.

65. Rogers, S. S., T. A. Waigh, and J. R. Lu. 2008. Intracellular microrheology of motile Amoeba proteus. *Biophys. J.* 94:3313–3322.

66. Duits, M. H. G., Y. Li, …, F. Mugele. 2009. Mapping of spatiotemporal heterogeneous particle dynamics in living cells. *Phys. Rev. E Stat. Nonlin. Soft Matter Phys.* 79:051910.

67. Robert, D., T.-H. Nguyen, …, C. Wilhelm. 2010. In vivo determination of fluctuating forces during endosome trafficking using a combination of active and passive microrheology. *PLoS One.* 5:e10046.

68. Weigel, A. V., B. Simon, …, D. Krapf. 2011. Ergodic and nonergodic processes coexist in the plasma membrane as observed by single-molecule tracking. *Proc. Natl. Acad. Sci. USA.* 108:6438–6443.

69. Manzo, C., J. A. Torreno-Pina, …, M. F. Garcia Parajo. 2015. Weak ergodicity breaking of receptor motion in living cells stemming from random diffusivity. *Phys. Rev. X.* 5:011021.

70. Witzel, P., M. Götz, …, D. Heinrich. 2019. Heterogeneities shape passive intracellular transport. *Biophys. J.* 117:203–213.

71. Marty, G., and O. Dauchot. 2005. Subdiffusion and cage effect in a sheared granular material. *Phys. Rev. Lett.* 94:015701.

72. Berthier, L., and W. Kob. 2007. The Monte Carlo dynamics of a binary Lennard-Jones glass-forming mixture. *J. Phys. Condens. Matter.* 19:205130.

73. Berthier, L., G. Biroli, …, D. R. Reichman. 2007. Spontaneous and induced dynamic fluctuations in glass formers. I. General results and dependence on ensemble and dynamics. *J. Chem. Phys.* 126:184503.

74. Berthier, L., G. Biroli, …, D. R. Reichman. 2007. Spontaneous and induced dynamic correlations in glass formers. II. Model calculations and comparison to numerical simulations. *J. Chem. Phys.* 126:184504.

75. Thompson, M. A., J. M. Casolari, …, W. E. Moerner. 2010. Three-dimensional tracking of single mRNA particles in *Saccharomyces cerevisiae* using a double-helix point spread function. *Proc. Natl. Acad. Sci. USA.* 107:17864–17871.

76. Stylianidou, S., N. J. Kuwada, and P. A. Wiggins. 2014. Cytoplasmic dynamics reveals two modes of nucleoid-dependent mobility. *Biophys. J.* 107:2684–2692.

77. Stuhrmann, B., M. Soares E Silva, …, G. H. Koenderink. 2012. Nonequilibrium fluctuations of a remodeling in vitro cytoskeleton. *Phys. Rev. E Stat. Nonlin. Soft Matter Phys.* 86:020901.

78. Toyota, T., D. A. Head, …, D. Mizuno. 2011. Non-Gaussian athermal fluctuations in active gels. *Soft Matter.* 7:3234–3239.

79. Grady, M. E., E. Parrish, …, D. M. Eckmann. 2017. Intracellular nanoparticle dynamics affected by cytoskeletal integrity. *Soft Matter.* 13:1873–1880.

80. Guan, J., B. Wang, and S. Granick. 2014. Even hard-sphere colloidal suspensions display Fickian yet non-Gaussian diffusion. *ACS Nano.* 8:3331–3336.

81. Ediger, M. D. 2000. Spatially heterogeneous dynamics in supercooled liquids. *Annu. Rev. Phys. Chem.* 51:99–128.

82. Müller, M. J. I., S. Klumpp, and R. Lipowsky. 2008. Tug-of-war as a cooperative mechanism for bidirectional cargo transport by molecular motors. *Proc. Natl. Acad. Sci. USA.* 105:4609–4614.

83. Charbonneau, P., J. Kurchan, …, F. Zamponi. 2017. Glass and jamming transitions: from exact results to finite-dimensional descriptions. *Annu. Rev. Condens. Matter Phys.* 8:265–288.

84. Angelini, T. E., E. Hannezo, …, D. A. Weitz. 2011. Glass-like dynamics of collective cell migration. *Proc. Natl. Acad. Sci. USA.* 108:4714–4719.

85. Garcia, S., E. Hannezo, …, N. S. Gov. 2015. Physics of active jamming during collective cellular motion in a monolayer. *Proc. Natl. Acad. Sci. USA.* 112:15314–15319.

86. Atia, L., D. Bi, …, J. J. Fredberg. 2018. Geometric constraints during epithelial jamming. *Nat. Phys.* 14:613–620.

87. Palamidessi, A., C. Malinverno, …, G. Scita. 2019. Unjamming overcomes kinetic and proliferation arrest in terminally differentiated cells and promotes collective motility of carcinoma. *Nat. Mater.* 18:1252–1263.

88. Chen, K., B. Wang, and S. Granick. 2015. Memoryless self-reinforcing directionality in endosomal active transport within living cells. *Nat. Mater.* 14:589–593.

89. Wattiaux, R., N. Laurent, …, M. Jadot. 2000. Endosomes, lysosomes: their implication in gene transfer. *Adv. Drug Deliv. Rev.* 41:201–208.

90. Watson, P., A. T. Jones, and D. J. Stephens. 2005. Intracellular trafficking pathways and drug delivery: fluorescence imaging of living and fixed cells. *Adv. Drug Deliv. Rev.* 57:43–61.

91. Vercauteren, D., J. Rejman, …, K. Braeckmans. 2012. On the cellular processing of non-viral nanomedicines for nucleic acid delivery: mechanisms and methods. *J. Control. Release.* 161:566–581.

92. Jhaveri, A., and V. Torchilin. 2016. Intracellular delivery of nanocarriers and targeting to subcellular organelles. *Expert Opin. Drug Deliv.* 13:49–70.

93. D. R. Lide and W. M. Haynes, eds 2009. CRC Handbook of Chemistry and Physics, 90th Edition CRC Press, Boca Raton, FL.

94. Montroll, E. W., and G. H. Weiss. 1965. Random walks on lattices. II. *J. Math. Phys.* 6:167–181.

95. Hughes, B. D. 1995. Random Walks and Random Environments: Random Walks. Clarendon Press, Oxford, UK.